SCI INSTITUTE
TECHNICAL REPORT

SCI INSTITUTE

Display of Vector Fields Using a Reaction-Diffusion Model

Allen R. Sanderson and Chris R. Johnson

Abstract:

Effective visualization of vector fields often rely on the size and density of the underlying mapping used to represent the field. In this paper, we introduce the use of a reaction-diffusion model to control the size, density, and placement of the vector field representation. The reaction-diffusion model is well known for its ability to form irregular spatiotemporal patterns, most notably spot patterns. We show that it is possible to create a mapping between the vector field and the parameters governing two different reaction-diffusion models to form a pattern at the correct orientation, size, and density to create an effective visualization. In addition, we show that it is possible to use the reaction-diffusion model to effectively visualize the uncertainty in the orientation of the vector field.

THE UNIVERSITY OF UTAH

Display of Vector Fields Using a Reaction-Diffusion Model

Allen R. Sanderson and Chris R. Johnson

Scientific Computing and Imaging Institute, University of Utah

Abstract

Effective visualization of vector fields often rely on the size and density of the underlying mapping used to represent the field. In this paper, we introduce the use of a reaction-diffusion model to control the size, density, and placement of the vector field representation. The reaction-diffusion model is well known for its ability to form irregular spatiotemporal patterns, most notably spot patterns. We show that it is possible to create a mapping between the vector field and the parameters governing two different reaction-diffusion models to form a pattern at the correct orientation, size, and density to create an effective visualization. In addition, we show that it is possible to use the reaction-diffusion model to effectively visualize the uncertainty in the orientation of the vector field.

1 Introduction

Visualizing vector field data is challenging because existing natural representations can not effectively visually convey significant amounts of information. Visualizing complex vector fields is important for many computational field applications, including air flow, fluid dynamics, wind and water currents in climate modeling, bioelectric fields in neuroscience, and magnetic fields in nuclear fusion. With such a diverse set of applications, many different techniques for visualizing vector fields have been developed [1, 3, 8, 9, 19, 21, 28, 30]. Each technique has their relative strengths and weaknesses in their ability to represent the vector magnitude, direction, orientation, uncertainty and critical points of the associated field.

For instance, the simplest method for displaying a vector field is to place glyphs representing the vector direction and magnitude at regular intervals. However, because of the scaling differences, overlap between the glyphs can occur. This produces visual clutter and occlusion often hiding areas of interest [23]. The problem is compounded when displaying data in three dimensions. Displaying normalized vector values can reduce the clutter but at a loss of information. Even when the visual clutter can be overcome, displaying vector fields using regular intervals may not be appropriate. This is because the grid spacing and orientation may not match the vector field.

More complicated techniques such as streamlines can provide powerful visual cues [10]. However, enough streamlines must be placed in the field to provide the cues without causing visual clutter. Streamlines can be selectively placed to reduce the clutter but at the cost of perhaps missing a critical area of interest [26].

With the exception of a glyph based method, no other technique is singularly able to visualize uncertainty in vectors fields. They must be combined with another technique such as color mapping or with another glyph to represent the uncertainty, In [16] Pang demonstrates several different glyphs for vector uncertainty. However, as a glyph based method it also succumbs to clutter and occlusion.

Given the shortcomings in many of the current flow visualization techniques, the main goal of this work was to develop an automated method that uses the vector magnitude, orientation and uncertainty to control the shape, size, orientation and density of the objects used to represent the vector field. At the same time, we wanted a method that would be mesh independent and produce a visualization that would be natural and pleasing to the eye. To achieve these goals, we have explored the use of a reaction-diffusion model for flow visualization.

2 Background and Previous Work

Visualizing vector fields has been a very active area of research for over a dozen years. During this time many different techniques have been developed. As such, it is not practical to review each technique. However, a very complete review can be found in [18]. Instead, we focus on three related areas for visualizing vector fields: the use of random patterns, selective placement, and reaction diffusion.

The use of random patterns for visualizing a vector field has been explored by van Wijk [27], Cabral [3], Shen [22], and others using either spot or white noise to form a dense representation of the vector field. By dense, we mean that there is value for each grid location. The resulting image has a natural brush stroke appearance. While this type of image is useful for showing flow orientation, it lacks information about the velocity magnitude and direction. These short comings have been addressed in various forms by adding directional cues, [22], velocity magnitude, [5, 13].

More recent work has focused on creating images that are less dense but still contain enough useful information about the flow. In [26] Turk proposes a method to bundle similar streamlines until an energy function is minimized. Once the function is minimized the streamlines can be replaced with variable sized curved arrows to show direction and magnitude. In [12] Kirby is able to achieve similar results using a random placement of variable sized arrows. Once an arrow is placed a Poisson distribution disk based on the vector magnitude is used to prevent other arrows from being placed near it. However, because the arrow represents just the value at a single location rather than a local region it is possible to miss critical points or have vector values occlude each other.

In computer graphics applications the use of a reaction-diffusion model has been used to generate texture maps [25, 29]. These types of textures are useful for forming patterns that are natural looking and are typically used on organic models such as animals. Turk explored the use of different reaction models to produce a variety of patterns [25]. At the same time, Witkin [29] used anisotropic diffusion to form different patterns. These patterns could be classified as either spot or stripe patterns.

Rather than forming the texture and then applying it to a model using a traditional texture mapping, Turk exploits the fact that a reaction-diffusion model can be used on an irregular grid. This allows textures to be created directly on the surface, avoiding any warping between model space and parameter space. It is possible to make use of this same property to texture isosurfaces, which are a very common visualization tool. In a similar vein, Chambers [4] used a reaction-diffusion model to generate a solid texture. This texture is then used on a surface or as a volume. Like Witkin, Chambers also use an anisotropic diffusion technique to form stripe patterns.

Although mentioned by Cabral [3] as a possibility, the first use of

a reaction-diffusion model for visualizing data was done by Kindlmann [11]. Like Chambers [4], Kindlmann created a solid texture using a reaction-diffusion model with anisotropic diffusion. Rather than randomly setting the diffusion values, Kindlmann used values from diffusion-weighted magnetic resonance images. This anisotropy formed elliptical "blobs," which were then volume rendered.

3   Reaction Diffusion

In 1952 Turing [24] proposed a reaction-diffusion model for describing the chemical process between two morphogens within a series of cells. Due to instabilities in the system, the morphogens both react and diffuse which changes their concentration within each cell. With time, the morphogens can form a stable pattern. The pattern formation is independent of the initial state of cells, they can be either homogeneous or random.

Turing described the reaction-diffusion of a two morphogen model as a set of nonlinear partial differential equations:

$$\frac{\partial a}{\partial t} = F(a, b) + d_a \nabla^2 a \tag{1}$$

$$\frac{\partial b}{\partial t} = G(a, b) + d_b \nabla^2 b \tag{2}$$

where a and b are the morphogens concentration; F and G are the functions controlling the production rate of a and b; d_a and d_b are the diffusion rates, and $\nabla^2 a$ and $\nabla^2 b$ are the Laplacians of a and b. Turing further defines F and G as:

$$F(a, b) = s(16 - ab) \tag{3}$$

$$G(a, b) = s(ab - b - B) \tag{4}$$

where a and b again are the morphogen concentration, B is the degrading rate of b, and s is the reaction rate, which Turing derives to be 1/16.

Previously we noted that the pattern formation was independent of the morphogen concentrations. This is not strictly true. For the state to change there must be some initial perturbation in the system. This perturbation can be from a non-uniformity in either the initial concentrations or the degrading rate, B. Current implementations, (e.g. Turk and Chambers), use a nonuniform degrading rate, whereas Turing perturbed the initial concentrations. A nonuniform degrading rate can be interpreted as being the natural variation within each cell.

After the system is put into motion, the morphogen concentrations will change until a dynamic equilibrium is reached and a stable pattern is formed. Although the pattern is stable, the morphogen concentration in each cell will continue to change. However, the change is statistically very small.

Turing's reaction equation is just one specific implementation of reaction-diffusion phenomena, there are others variants that give similar results. For example, Pearson [17] describes a reaction model due to Gray and Scott [6, 7] that has the form:

$$F(a, b) = -ab^2 + F(1 - a) \tag{5}$$

$$G(a, b) = ab^2 - (F + k)b \tag{6}$$

where F is the feed rate and k is the degrading rate. There are other similar variations that can be found in the literature such as those in [15] and in Chamber's cellular automata [4].

3.1   Mapping the Reaction-Diffusion Kinetics

In order to use a reaction-diffusion model for visualization, a mapping must be established between the vector field and the reaction-diffusion model. There are three possibilities, a mapping between the field and the reaction kinetics, a mapping between the field and the diffusion kinetics, or a combination of both. It has been well documented that reaction-diffusion models are highly numerically unstable if not properly "tuned." As such, we have currently focused on finding a mapping for either reaction or diffusion kinetics but not both.

3.2   Reaction Kinetics

Pearson [17] maps the patterns formed using a Gray-Scott reaction-diffusion model as a function of the two rates, F and k, in the reaction kinetics. These patterns range from finger prints to spots, with a large variety in between. We found similar results with Turing's reaction kinetics, ranging from smears to spots and lines. However, both were very sensitive to their initial conditions as it was very easy to produce an unstable system. The variety in patterns and instability is due to the nonlinearity of the reaction kinetics. Because of this, we chose not to pursue a mapping between the vector field and the reaction kinetics. However, when acceptable values for the rates are used, the reaction kinetics for both models form a stable pattern.

3.3   Diffusion Kinetics

The diffusion kinetics as written in Equation (1) has just one free parameter, the diffusion rate. Changing the diffusion rate changes the size of the pattern formed. Others have noted similar results but as a function of the reaction rate. Strictly speaking, it is not the reaction or the diffusion rate that changes the size, but rather their relative difference. For simplicity and clarity, we keep the reaction kinetics just a function of the cell concentration varying only the reaction-diffusion kinetics.

Since the diffusion rate can be used to control the size of the pattern this provide an ideal mapping to a scalar value, such as the vector magnitude. The other mapping we wish to establish is one for orientation. Previously, we stated that there was only one free parameter in the diffusion equation. This is the case for isotropic diffusion. If we relax this condition and use anisotropic diffusion, we are able to create a broader range of patterns. The diffusion equation becomes:

$$\frac{\partial a}{\partial t} = F(a, b) + (\nabla \cdot D_a \nabla)a, \tag{7}$$

where D_a is a diffusion tensor matrix and has the form:

$$D_a = \begin{pmatrix} D_{xx} & D_{xy} \\ D_{yx} & D_{yy} \end{pmatrix}. \tag{8}$$

Combining the diffusion matrix with a discrete finite difference approximation of the generalized Laplacian convolution mask yields:

$$(\nabla \cdot D_a \nabla)a = \mu \begin{pmatrix} -D_{xy} & 2D_{yy} & D_{xy} \\ 2D_{xx} & -4(D_{xx} + D_{yy}) & 2D_{xx} \\ D_{xy} & 2D_{yy} & -D_{xy} \end{pmatrix} * a \tag{9}$$

where we have set $D_{xy} = D_{yx}$ and μ is a space constant. For complete details of the derivation of Equation (9) see [11] and [29].

By manipulating the diffusion matrix coefficients it is possible to create an oriented pattern. Witkin [29] takes this approach for creating 2D texture patterns. In our case, we are interested in using patterns that match the vector field orientation. This is accomplished

by applying a two dimensional rotation matrix to an anisotropic diffusion matrix that produces an oriented pattern. The rotation matrix provides the mapping needed for the vector orientation. In addition to the rotation matrix, we apply a scaling matrix which provides the pattern size change. With this control, we now have our desired mapping between the vector field and the reaction-diffusion model.

3.4 Image Formation

Creating a reaction-diffusion image is done using a forward Euler integration on the discrete versions of Equations (1) and (2) until a dynamic equilibrium state is reached at which time a stable pattern will have formed. We have found that using a time step of 0.5 provided a balance between numerical stability and accuracy and the pattern formation.

Up to this point we have described the use of a reaction-diffusion model for generating non-specific patterns. We now limit ourselves to generating patterns that can be used for visualizing flow. The most common pattern formed using a reaction-diffusion model is a spot pattern. Figure (1) shows two similar spot patterns created with the Turing and Gray-Scott models, respectively. See Appendix 1 for the parameters used to form the patterns.

A comparison of these two figures shows that the spot placement is balanced. That is, there is a uniform density of spots with equal spacing around them. This balancing process can be observed during the integration process when a spot begins to form in an area of lower concentration. Other near-by spots adjust themselves so they are not too close to the newly formed spot. Sometimes this adjustment may be in the form of a change in the position of the spots or by one or more of the spots disappearing with its concentration being absorbed by remaining spots. This natural organization is one of the properties of reaction-diffusion equations that makes them very useful for visualization purposes.

A further comparison shows that although the spot sizes are approximately the same in both images, the Gray-Scott pattern has a denser packing than the Turing pattern. The other item of interest is that even though the diffusion is isotropic, the spots in the Turing model are not as symmetric as those in Gray-Scott model. This non-uniformity is proportional to the variance of the degradation factor, B. The greater the variance, the greater the chance for this asymmetry to appear in the spots which may cause undesirable effects.
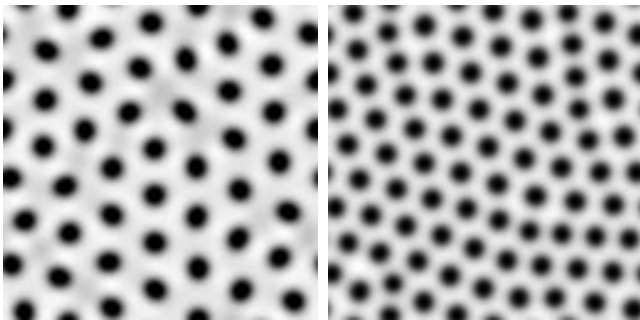

Figure 1: *Turing model visualization of random spots and Gray-Scott model visualization of random spots.*

Circular spots alone do not show orientation or magnitude. As discussed previously, to give an orientation we apply an anisotropic diffusion matrix. This compresses the spots so they have an elliptical shape. Next, we rotate the diffusion matrix so that the ellipse's major axis is aligned with the vector field. Finally, we apply a diffusion scalar, d to reflect the magnitude of the vector. This matrix

is formed for each vector in the flow field. Figures (2) and (3) show the anisotropic diffusion applied to the Turing and Gray-Scott models for a vector field at 45 degrees with a random variation in the magnitude.
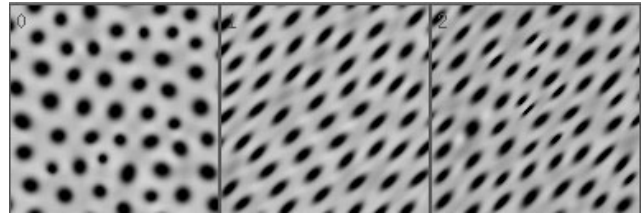

Figure 2: *Turing model visualization of a vector field with a) random magnitude b) constant orientation c) magnitude and orientation.*
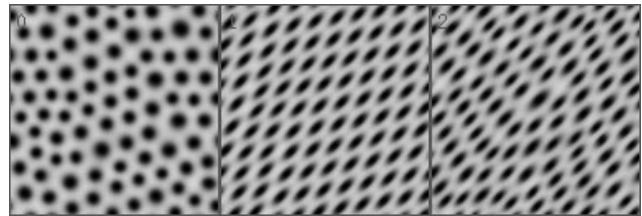

Figure 3: *Gray-Scott model visualization of a vector field with a) random magnitude b) constant orientation c) magnitude and orientation.*

3.5 Uncertainty Measurements

In the previous examples, we have fixed the amount anisotropy in the diffusion matrix. However, this need not be the case. By allowing the amount of anisotropy to vary, we have another variable that can be mapped. We define the amount of anisotropy to be the ratio of the diffusion matrix eigenvalues.

When the amount of anisotropy is small, the spot formed is cylindrical. Whereas when the anisotropy is high, the spot formed is elliptical and at times, almost to the point of being a thick line. This difference is very well suited to mapping an orientation uncertainty. When the orientation uncertainty is very small the spot is very elliptical, reflecting a precise orientation. When the uncertainty is very high, the spot is more cylindrical, reflecting the uncertainty in the orientation. This is demonstrated in Figure (4).

4 Results and Discussion

The first application of our reaction-diffusion models was to visualize vector flow data with a set of idealized flow fields. Our goal was to see if it was possible to capture the nature of different types of vector fields commonly visualized. These fields included circular flow, Figure (5); flow at a saddle and sink; Figure (6), flow around a cylinder, and the flow field from an electrostatic charge field, Figure (7). The flow for each field changed smoothly over both the orientation and magnitude. In each case the flow can easily be discerned as the ellipsoidal spots are properly oriented within the field. In the case of the circular, saddle, and source fields, a change in the vector magnitude occurs as the field moves away from the center and is shown by a corresponding change in the spot size. However, in Figure (6), the Turing images have several spots that did not form very
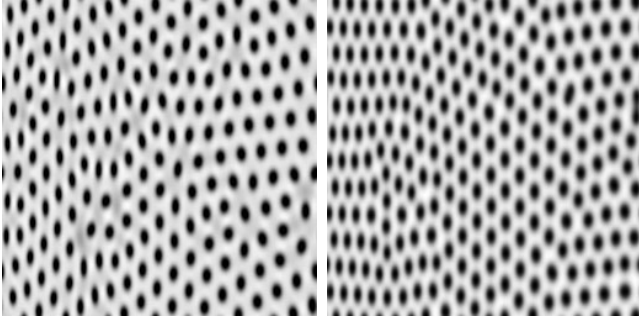
Figure 4: *Turing model visualization of orientation uncertainty and Gray-Scott model visualization of orientation uncertainty. The orientation uncertainty increases from left to right across the image.*

Figure 6: *Turing model visualization of a saddle vector field and a sink vector field.*

well, appearing to be smeared together. This is due to the variance of the degradation factor, B.

Figure 5: *(a) Turing model visualization of a circular vector field and (b) Gray-Scott model visualization of a circular vector field.*

Figure 7: *Gray-Scott model visualization of the flow around a cylinder and a visualization of an electrostatic charge field.*

Figures (8) and (9) show the Turing and Gray-Scott reaction-diffusion models for visualizing an idealized flow that contains three saddles and two vortices. In an informal observer study we found that it was easier for observers to follow the flow in the Turing model visualization, yet easier to pick out critical points in the Gray-Scott model visualization. This observation is probably due to the density of the spots. Denser arrays of spots make it easier to view critical points, but in this case also tended to make it more difficult to discern the overall flow pattern. Whereas the opposite was true when the spot density was reduced.

One of the unique features of using a reaction-diffusion model is that the pattern formation, although random, naturally aligns itself along the flow, forming a rough streamline. Further, when the flow is curved the spots are not perfectly elliptical, they are more of a bean shape. This is due to the oriented anisotropy for each vector influencing the overall spot shape. The ansiotropy has another benefit, in that as the pattern develops faint streaks emanate from the ends of the spots. These streaks act to connect the spots into rough streamlines, further aiding in visualizing the flow.

This aligning, bending, and streaking all give the observer cues as to where laminar flow occurs. But locations of turbulence and critics points may also be of interest. This is another area where the reaction-diffusion model is able to give a visual cue. For instance, at locations where the flow is diverging, the spots are no longer elliptical but assume an odd shape. If the flow is diverging equally in all directions the spots would be circular. As such, oddly shaped or circular spots could indicate either turbulence, a critical point, or where the uncertainty of the orientation is large. These are loca-
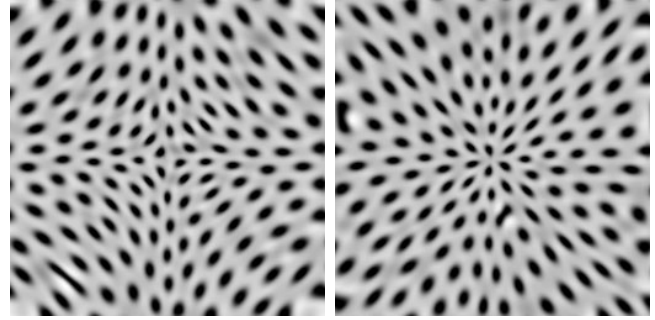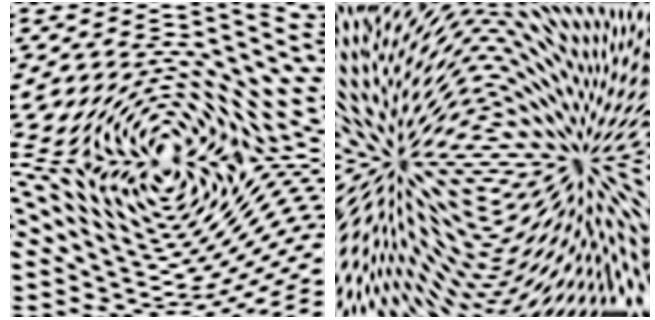
tions that the observer may want to further inspect. For instance, in Figures (8) and (9) the spots are elliptical in shape and are aligned with the flow throughout the image except at the saddle points.

We have shown that it is possible to view different types of flow using a reaction-diffusion model, one question that arises is: what is the minimum resolution required for individual features to be seen? By its nature, the process of diffusion acts to smooth, lowering high concentrations and raising low concentrations. As such, it is possible to lose individual features that are significantly different than their neighbors.

To determine the minimum resolution at which features can be seen, we oversampled a vector field until it was possible to see the impact of a single vector that was significantly different in both magnitude and orientation than its surrounding, otherwise constant neighbors. This is demonstrated in Figures (10) and (11) for both magnitude and orientation separately. It is not until there is an over sampling of four times the original that the magnitude will significantly impact its neighbors to be visually of notice. Similarly, it takes an over sampling of eight times for the angle to impact its neighbors. Unfortunately, for large vector fields, over sampling is not always practical since it may require significantly more computational resources than available. As such, when visualizing a vector field without oversampling features less than four to eight nodes in size may be smoothed out.

We now apply the Gray-Scott reaction-diffusion model to a numerical simulation of the nonlinear magneto-hydrodynamics (MHD) that occur in the DIII-D tokamak nuclear fusion reactor. The vector field shown in Figures (12-14) is a two dimensional slice of the magnetic field in the Tokamak reactor. In Figure (12), just the magnitude of the vector field is visualized with no orientation information. This gives a good example of how this technique can
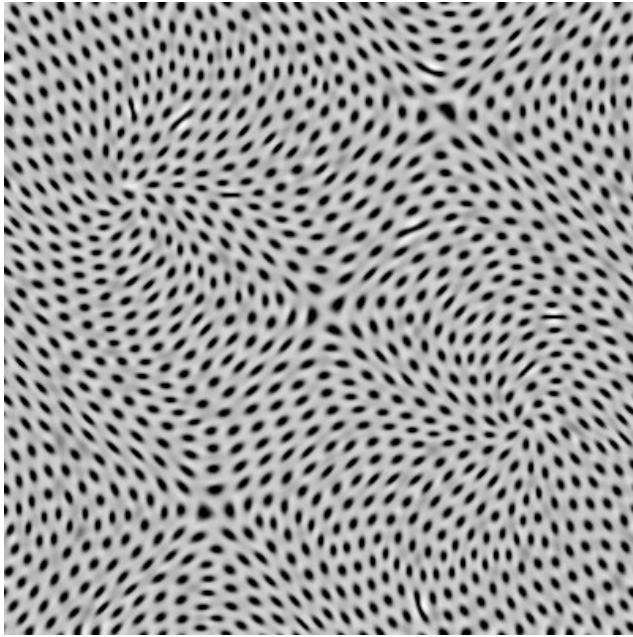
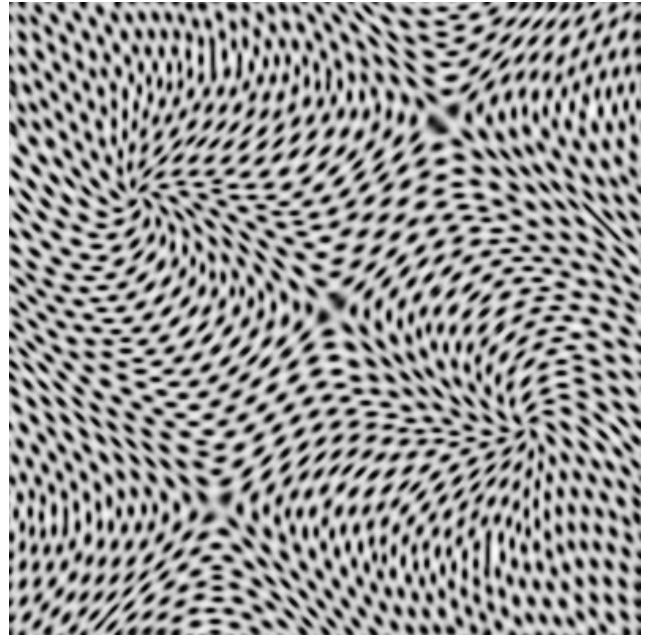Figure 8: *Turing model visualization of multiple flow types.*

Figure 9: *Gray-Scott model visualization of multiple flow types.*

be use for visualizing scalar data. Figure (13) is the same vector field except normalized. Finally, in Figure (14), the vector field is shown with both magnitude and orientation.

Figures (15) and (16) show visualizations of the plasma velocity for the same simulation set using the Turing and the Gray-Scott models, respectively. In these cases, the flow is much more erratic, though it is still can be discerned. Comparing these two images demonstrates the effectiveness of producing a pattern at the proper density. It is much easier to follow the flow in the Gray-Scott model which has a denser pattern than the Turing model. However, this is not always the case, as was demonstrated in Figures (8) and (9).

4.1 Comparison with Other Flow Visualization Techniques

The reaction diffusion images provide a very good vector visualization technique. But is it better than some of the current techniques? For instance, this technique alone does not show the flow direction. This is often a very import cue in analyzing vector data. We have addressed this issue by overlaying a small arrow on top of each spot to show the flow direction, as shown in Figure (17). The arrow direction is determined using the average value of the vectors surrounding the centroid of the spot. The centroid is determined using standard image processing techniques of thresholding and thinning [20].

We now compare the reaction-diffusion images with three different common visualization techniques. Figure (18) shows vector glyphs at regular intervals [23], Figure (19) shows a line integral convolution [3], and Figure (20) shows optimized streamlines [26].

Placing glyphs at regular intervals is much simpler and quicker than using a reaction-diffusion model, but as previously discussed occlusion is a problem, as such, the vectors are normalized. Using a reaction-diffusion model overcomes the occlusion problem since the spots have a packing that is based upon the vector magnitude. Another problem with regular intervals is that they may mislead the eye due to the formation of a pattern that may not be part of actual vector flow. Conversely, the reaction-diffusion model form spots in
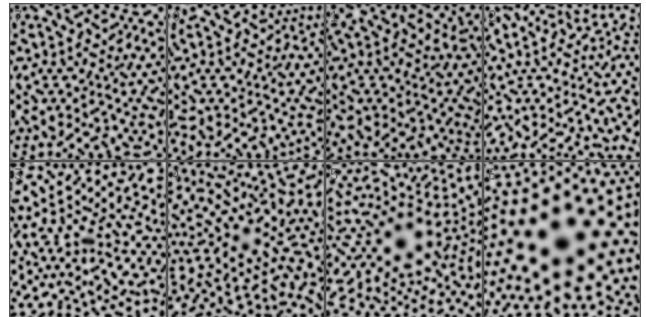

Figure 10: *Effect of a single value on the spot size with an oversampling of 0, 1, 2, 4, 8, 16, 32, and 64 times. The image is 128x128.*

a pattern that follows the natural structure of the flow.

When compared to LIC, both techniques visualize the flow in a manner that is natural and easy to observe by producing a dense image representation of the flow field. With reaction-diffusion images, different models will produce spots at different densities. The less dense the spots, the greater the chance that areas of interest may be missed. However, images with a high density of spots may be difficult to view because of the Moray patterns that can form. As such, the density of the spots is a critical component for an effective reaction-diffusion flow visualization. Currently, the only way to control the density is by using different reaction-diffusion models.

Unlike LIC images, which do not contain magnitude information, the reaction-diffusion model is able to naturally incorporate magnitude information into the visualization. Including the magnitude greatly enhances the visualization. LIC images, and other noise based techniques, can be extended to show the magnitude but these techniques do so at a loss in flow detail because of blurring used to emphasize the magnitude [5, 14].

Next, we compare the reaction-diffusion image to a visualization using the image guided streamline technique developed by
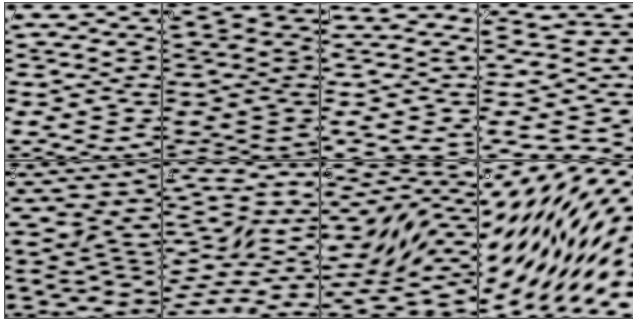
Figure 11: *Effect of a single value on the spot orientation with an oversampling of 0, 1, 2, 4, 8, 16, 32, and 64 times. The image is 128x128.*
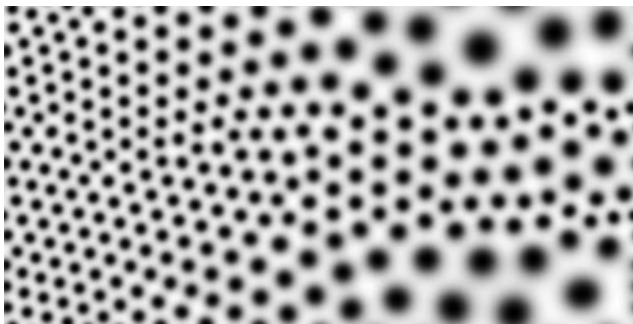

Figure 13: *Gray-Scott reaction-diffusion visualization of a MHD Magnetic vector field. Orientation only.*

Figure 12: *Gray-Scott reaction-diffusion visualization of a MHD Magnetic vector field. Magnitude only.*

Figure 14: *Gray-Scott reaction-diffusion visualization of a MHD Magnetic vector field. Magnitude and orientation.*

5 Conclusions and Future Work

We have introduced the use of a reaction-diffusion model that can produce patterns with different shapes, sizes, and orientations for visualizing vector fields. We are able to control the pattern formation by mapping two of the vector field components, orientation and magnitude, to the diffusion kinetics. In addition, we also can map an orientation uncertainty to the diffusion kinetics. This mapping produces a spot pattern that is highly representative of the vector field. Further we are able to control the density of the pattern through the use of two different models. While we are not able to directly map the direction of the field, we can augment the reaction-diffusion visualization with directional information.

The principle advantage of the reaction-diffusion model over existing flow field visualization techniques is that the pattern size and density that naturally arises from the reaction-diffusion model accurately represents the underlying vector field. Further, the shape of the pattern (e.g. the spots) contains not only orientation and magnitude information but also can contain uncertainty information.

Future work includes extension of the reaction-diffusion algorithm to three dimensions. The reaction kinetics remain the same only the diffusion kinetics must be extended. The output is a three dimensional texture that can be volume rendered using various techniques or applied to two dimensional surfaces. The image generated would have similar characteristics to those generated by Kindlmann [11] and Chambers [4] and unfortunately suffer from the same visualization problems.

The post image formation addition of the direction vector is really a combination of two independent techniques, patterns and glyphs. It may be possible to combine our reaction-diffusion model with other techniques to achieve a better visualization. For instance, Shen's dye advection would be suited for interactively showing the

Turk [26]. Both techniques are similar in that they both are able to show direction, magnitude, and orientation. However, the reaction-diffusion technique is better able to represent the magnitude than the image guided technique. That is, the image guided technique suffers from the same occlusion problem as the vector glyphs. Although Turk allows the arrows to be scaled, the dynamic range is compressed so much that it is difficult to see any difference in magnitudes.

One of the drawbacks to using a reaction-diffusion model compared to the other techniques is the computational expense. The patterns take many iterations to form and become stable, whereas it is possible to produce LIC images at interactive rates [2]. Some of this expense can be reduced since the computation can be parallelized and other, faster integration methods can be employed.

One of the greatest benefits to using a reaction-diffusion model is the ability to seamlessly integrate the uncertainty measurements in with the model. None of the other techniques, with the exception of vector glyphs, are able to show uncertainty as part of their representation [16]. Although vector glyphs can show uncertainty, they still have difficulties with occlusion.

One problem that can occur during pattern formation is that spots can form and fail to separate, as shown in Figure (13). Where this happens is random and appears to be dependent on the initial conditions. We have observed that it tends to happen more frequently with smaller spots, especially those which are either horizontally or vertically oriented and when mapping just a single component.
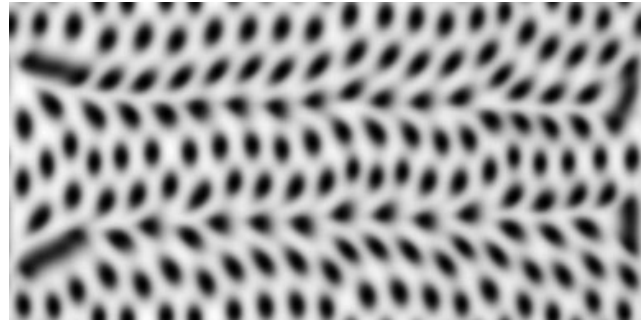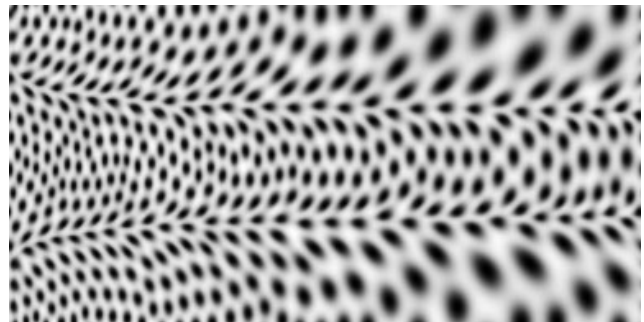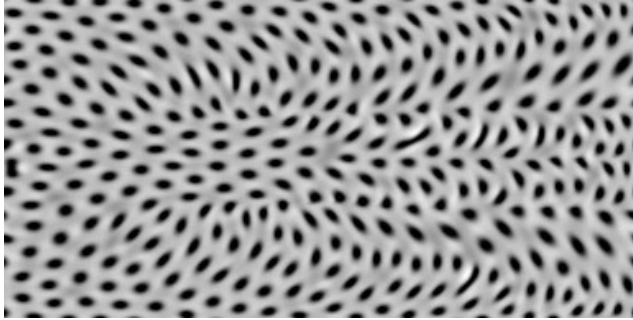
Figure 15: *Turing reaction-diffusion visualization of a MHD plasma velocity vector field.*

Figure 17: *. Overlayed direction arrows on Figure (13).*

Figure 16: *Gray-Scott reaction-diffusion visualization of a MHD plasma velocity vector field.*

Figure 18: *Uniform sampled vector glyph image of the same vector field used in Figure (14).*

7.1 Turing Model Parameters:

$a = 4.0$
$b = 4.0$
$D_a = 1.0 / 4.0$
$D_b = 1.0 / 16.0$
$B = 16.0 \pm 1\%$
$s = 1.0 / 64.0$

7.2 Gray-Scott Model Parameters:

$a = 0.50 \pm 1\%$ for the central 12×12 area, 1.0 else where.
$b = 0.25 \pm 1\%$ for the central 12×12 area, 0.0 else where.
$D_a = 2.0\text{e-}5$
$D_b = 1.0\text{e-}5$
$F = 0.0300$
$k = 0.0625$
For the Gray-Scott model it is necessary to normalize the diffusion values. For this we assume a cell area of 0.001.

flow direction over the spots [22]. Rather than have the dye move through the whole image only spots would change their color. Combinations of other techniques are certainly feasible. However, it may be possible to use of other reaction-diffusion patterns that have both orientation and direction. This would eliminate the need for combining it with another technique.

Finally, there are a number of perceptual issues that require further investigation, including a formal user study to determine the effectiveness of the reaction-diffusion visualization technique in comparison to other flow field visualization techniques. One area of particular interest is quantifying the effectiveness of the natural patterns that form from using a reaction-diffusion model.

6 Acknowledgments

7 Appendix

One of the difficulties in using a reaction-diffusion model is the inherent instability of the system. Below are the parameters used to obtain stable patterns in the Turing and Gray-Scott models shown in Figure (1).
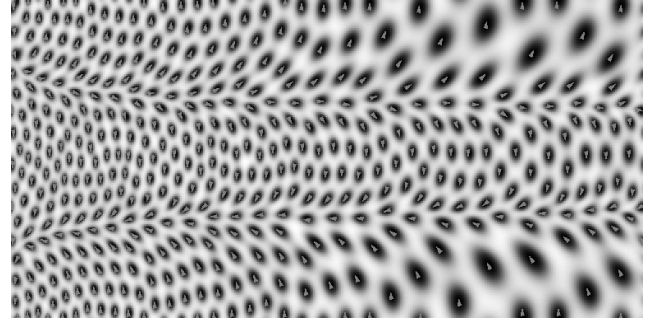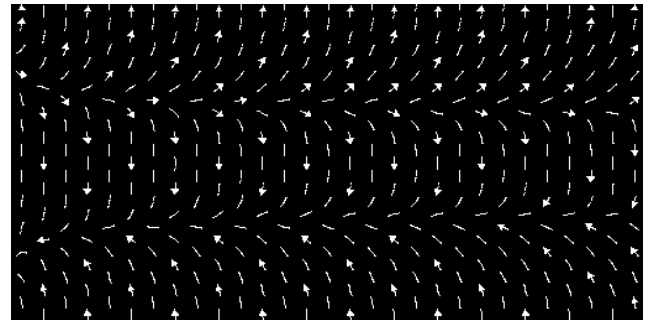
References

[1] D.C. Banks and B.A. Singer. A predictor-corrector technique for visualizing steady flow. *IEEE Transactions on Visualization and Computer Graphics*, 2:151–163, 1995.

[2] U. Bordoloi and H.W. Shen. Hardware accelerated interactive vector field visualization: A level of detail approach. *Computer Graphics Forum*, 21(3), 2002.

[3] B. Cabral and C. Leedom. Imaging vector fields using line integral convolution. In *Proceedings of SIGGRAPH 93*, pages 263–270. ACM SIGGRAPH, 1993.

[4] P. Chambers and A. Rockwood. Visualization of solid reaction-diffusion systems. *IEEE Computer Graphics and Applications*, pages 7–11, 1995.

[5] W.C. de Leeuw and J.J. van Wijk. Enhanced spot noise for vector field visualization. In *IEEE Visualization 95 Proceedings*, pages 233–239, 1995.
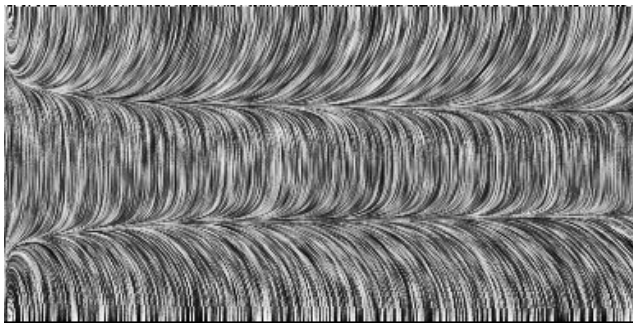
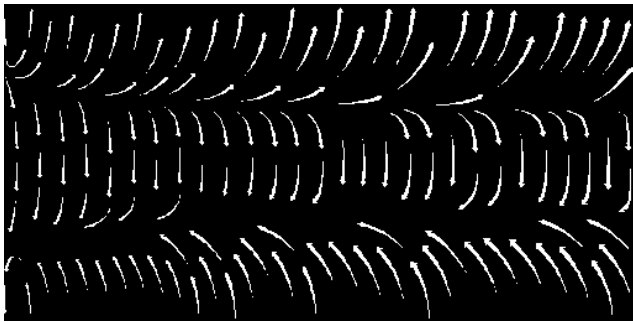Figure 19: *LIC image of the same vector field used in Figure (14).*

Figure 20: *Optimized streamlines generated by Turk's algorithm of the same vector field from (14).*

[6] P. Gray and S.K. Scott. Sustained oscillations and other exotic patterns of behaviour in isothermal reactions. *J. Phys. Chem.*, 59:22–32, 1985.

[7] P. Gray and S.K. Scott. *Chemical Oscillations and Inestability: Non-linear Chemical Kinetics*. Oxford University Press, 1990.

[8] J. Helman and L. Hesselink. Visualizing vector field topology in fluid flows. *IEEE Computer Graphics and Applications*, May 1991.

[9] L. Hultquist. Constructing stream surfaces in steady 3D vector fields. In *Proceedings of IEEE Visualization '92*, pages 171–177. IEEE Computer Society Press, 1992.

[10] D.N. Kenwright and G.D. Mallinson. A 3-D streamline tracking algorithm using dual stream functions. In *IEEE Visualization 92*, pages 62–68, 1992.

[11] G.L. Kindlmann and D.M. Weinstein. Strategies for direct volume rendering of diffusion tensor fields. *IEEE Trans. Visualization and Computer Graphics*, 6(2):124–138, 2000.

[12] R.M. Kirby, H. Marmanis, and D.H. Laidlaw. Visualizing multivalued data from 2d incompressible flows using concepts from painting. In *Proceedings of the IEEE Visualization 99*, 1999.

[13] M.H. Kiu and D.C. Banks. Multi-frequency noise textures for lic. In *Proceedings of IEEE Visualization 96*, pages 121–126. IEEE, 1996.

[14] Ming-Hoe Kiu and David C. Banks. Multi-frequency noise for LIC. In Roni Yagel and Gregory M. Nielson, editors, *IEEE Visualization '96*, pages 121–126, 1996.

[15] J.D. Murray. *Mathematical Biology*. Springer-Verlag, New York, 1989.

[16] A.T. Pang, C.M. Wittenbrink, and S.K. Lodha. Approaches to uncertainty visualization. *The Visual Computer*, 13(8):370–390, 1997.

[17] J.E. Pearson. Complex patterns in a simple system. *Science*, 261:189–192, 1993.

[18] F. Post, B. Vrolijk, H. Hauser, R.S. Laramee, and H. Doleisch. Feature extraction and visualization of flow fields. *Eurographics 2002*, pages 69–100, 2002.

[19] F.J. Post, T. van Walsum, Post F.H., and D. Silver. Iconic techniques for feature visualization. In *IEEE Visualization 95 Proceedings*, pages 288–295, 1995.

[20] A. Rosenfeld and A.Kak. *Digital Picture Processing*. Academic Press, 1982.

[21] C. Schroeder, W. Volpe and W. Lorensen. The stream polygon: A technique for 3D vector field visualization. In *IEEE Visualization '91*, pages 126–132. IEEE Press, 1991.

[22] H.W. Shen, C.R. Johnson, and K.L. Ma. Global and local vector field visualization using enhanced line integral convolution. In *Symposium on Volume Visualization*, pages 63–70. IEEE Press, 1996.

[23] E.R. Tufte. *The Visual Display of Quantitative Information*. Graphics Press, Cheshire, Conn., 2nd edition, 2001.

[24] A.M. Turing. The chemical basis of morphogenesis. *Phil. Trans. Roy. Soc. Lond.*, B237:37–72, 1952.

[25] G. Turk. Generating textures on arbitrary surfaces using reaction-diffusion. *Computer Graphics (SIGGRAPH)*, 25(4):289–298, 1991.

[26] G. Turk and D. Banks. Image-guided streamline placement. *Computer Graphics (SIGGRAPH)*, pages 453–460, 1996.

[27] J.J. van Wijk. Spot noise: Texture synthesis for data visualization. *Computer Graphics*, 25(4):309–318, 1991.

[28] R. Westermann, C. Johnson, and T. Ertl. A level-set method for flow visualization. In *IEEE Visualization 2000*, pages 147–154, Salt Lake City, 2000. IEEE Computer Society.

[29] A. Witkin and Mi. Kass. Reaction-diffusion textures. *Computer Graphics (SIGGRAPH)*, 25(4):299–308, 1991.

[30] M. Zockler, D. Stalling, and H-C. Hege. Interactive visualization of 3D-vector FIelds using illuminated stream lines. In *Visualization '96*, San Francisco, CA., 1996. IEEE Press.